ORIGINAL ARTICLE

On Digitally Identifying the Very Low-Lying Amplitude Deviation and Rhythmic Irregularities in EEG Signal for Epileptic Seizure Detection and Analysis

Khakon Das [1], Ashish Khare [1*], Nilesh Anand Srivastava [1], Shankar Prasad Saha [2]

[1] *Department of Electronics & Communication, University of Allahabad, Prayagraj-211002, Uttar Pradesh, India*

[2] *Department of Neurology, Institute of Neurosciences Kolkata, Kolkata-700017, India*

*Corresponding Author: Ashish Khare

Email: khare@allduniv.ac.in

Received: 05 August 2024 / Accepted: 30 December 2025

Abstract

Purpose: Recent studies signify that epilepsy has become a significant burden to society due to its unpredictable nature and high cost of treatment. It has been observed that an integrated neural investigation system is required to aid epileptologists for early diagnosis as well as long-term monitoring of patients. Electroencephalogram (EEG) plays a significant role in studying the brain's electrical activity, such as in epilepsy. An epileptic EEG signal has four necessary distinctive characteristics: sudden changes in signal, amplitude deviations, electrocerebral negativity, and formation of physiological fields by affected EEG channels.

Materials and Methods: In this paper, we propose an automated system for epileptic seizure prediction using the above-mentioned characteristics. In the proposed system, the very low-lying amplitude deviation and rhythmic irregularities were identified in the EEG signal. The proposed work focuses on extracting features from EEG signals and brain structure. This includes analyzing sudden changes in the foreground and background of the signal, detecting amplitude deviations in EEG signals even at very low levels. Additionally, the study focuses on highlighting the electrocerebral negativity nature of the EEG signals and exploring the formation of physiological fields between multiple electrodes. Also, the proposed system provides dual execution mode (detection and analysis) and is able to predict the epileptic seizure waveforms, classification of epileptic seizure, and specific brain regions that will be affected by upcoming seizures.

Results: The proposed system accurately identifies various seizure waveforms in EEG signals of the primary dataset and achieves an excellent performance (92.66% accuracy, 94.86% F1 score) in the prediction of epileptic seizures, and in the case of secondary dataset, it shows a maximum of 100% accuracy.

Conclusion: The advantage of the proposed system lies in the generation of a detailed report on upcoming seizure location and nature to the seizure, which mitigates patient life risks. This advancement could lead to substantial improvements in the field of neuroscience.

Keywords: Classification; Detection; Electroencephalogram; Epilepsy; Seizure; Segmentation.

DOI:

1. Introduction

Epilepsy is among the most common non-communicable chronic diseases in humans. It affects around 50 million people worldwide. It has been estimated that the majority of people affected by epilepsy live in low and middle-income countries. As a result, about 25% of epileptic patients can not have access to any convenient treatment [1]. Neurological disorder (Epilepsy) affects people of all ages, and it increases the risk of premature death by almost three times compared to normal people [2]. Seizure is an irregular electrical activity experienced in the human brain during epilepsy [3]. It causes loss of consciousness [4-5], vision disturbance [4-5], hearing difficulty [4-5], or even an entire body convulsion [4–6]. Usually, most of the people are not aware of seizure occurrence, due to its uncertain nature, which increases the risk of permanent brain damage [2]. If an instant epileptic seizure detector is available, then people living with epilepsy can be treated with the appropriate anti-seizure medicines at the right time.

1.1. Background

Recently, numerous methodologies have been developed for the detection and analysis of epilepsy from EEG signals [7, 8]. Wavelet-based EEG processing for computer-aided seizure detection and epilepsy diagnosis was performed in [7]. Further, a classification of EEG signal into the various phases (parts) plays a significant role in the detection of epileptic seizure patterns. Vesna Zeljković *et al.* [9] implemented an algorithm that converts a 1D EEG signal into a 2D signal-image to detect snake-like shapes within the image. In addition, they employed a mean value-based approach to identify seizures related to epilepsy, specifically from the pre-ictal phase of the EEG. Usman *et al.* [10] had developed a method to detect the pre-ictal phase 23.6 minutes earlier than seizure occurrence. This was performed using Empirical Mode Decomposition (EMD) for pre-processing and has extracted time and frequency domain features for training the proposed prediction model [10]. Further, a significant improvement has been made by Acharya *et al.* [11], who successfully identified the normal, ictal, and pre-ictal phases of the EEG using four entropy features (Approximate Entropy (ApEn), Sample Entropy (SampEn), Phase Entropy 1 (S1), and Phase Entropy 2 (S2)). These features were fed to seven different classifiers: Fuzzy Sugeno Classifier (FSC), Support Vector Machine (SVM), K-Nearest Neighbour (KNN), Probabilistic Neural Network (PNN), Decision Tree (DT), Gaussian Mixture Model (GMM), and Naive Bayes Classifier (NBC). Moreover, the Fuzzy classifier was able to differentiate the three classes with a high accuracy of 98.1% [11]. Further, an SVM classifier-based technique, based on temporal correlation, has been proposed by Parvez *et al.* [12] to detect the inter-ictal and ictal phases of EEG signals. In continuation, the authors of [9, 11, 13, 14] have further discussed the various parts of EEG signals like ictal, normal, pre-ictal, interictal, and post-ictal in their research works. The patterns associatedwith epileptic seizures, such as spike and waves, and spikes have been interpreted by Zeljkovi´c *et al.* [9], and Basiri *et al.* [14]. Furthermore, Faust *et al.* [15] discussed a set of wavelet-based features like Haar, Spline, Morlet, and Daubechies (db) for detecting seizures from EEG signals. In [16], the authors detected temporal lobe seizures using various features such as Brain Symmetry Index (BSI), spectral measures, phase synchronization, and non-linear methods. Based on this study, it is clear that a lot of features exist for epileptic seizure detection. Now it became important to select the most relevant and optimal number of features from the pool of features to reduce the complexity of the algorithm. In previous studies [16, 17], a detailed feature selection method for detecting and localizing epileptic seizures is presented. Among all the features outlined in [16], BSI stands out as the most effective feature for detecting temporal lobe seizures with a minimal (0.55) false alarm rate. Seizure detection using an SVM classifier and Hilbert-Huang transform achieved a 79.7% detection rate on the ictal part of EEG for epileptic seizures. Nadim Mohamed [18], in his research, focused on the inter-ictal activity of the EEG signal for seizure identification using a neural network and achieved 95.1% classification accuracy. While the early-stage algorithms had moderate sensitivity and specificity rates, recent research has shown excellent sensitivity and specificity [19, 20]. However, less attention has been paid to obtaining the optimal solution in epileptic seizure detection. Here, the term “optimal solution” refers to the minimum number of features and minimum time to detect the epileptic seizure. In this

paper, a system for digitally identifying the very low-lying amplitude deviation and rhythmic irregularities in the EEG signal has been proposed. It considers a small set of highly correlated features of the per-ictal phase of the EEG signal, which make it an optimal solution in terms of features. On the other hand, the time advantage is achieved by using the pre-ictal phase of the EEG signal, which may greatly help to predict epileptic seizures.

1.2. Contributions

- In this proposed work, the epileptic seizure wave-forms (e.g., sharp spike, thick spike, sharp spike & wave, and, thick spike & wave) have been recognized from the pre-ictal part of the EEG signal, which brings the time advantage.
- The proposed system is capable of predicting the seizure in advance from the actual time of the seizure occurrence, because it uses the pre-ictal phase to detect epileptic seizure which occur before the ictal phase.
- The proposed system has two modes: one is detection mode for seizure detection, and the other is analysis mode for detailed reporting.
- The detection mode of the system conveys a warning message regarding epileptic seizure occurrence.
- Analysis mode of the proposed model generates a report describing the location of upcoming seizures and pattern of the seizure wave-forms, which eventually helps the neurologists to analyze and make planning of treatment for the patient.

This paper has been divided into four sections. Section 1 contains the introduction and the related work. Section 2 describes the design methodology. Next, Section 3 demonstrates the results and discussions, and the work has been concluded in Section 4.

2. Materials and Methods

2.1. Design Methodology

This section describes the proposed methodology in detail. A conceptual model of the proposed design is shown in Figure 1, which shows all the major steps involved in the proposed system. Firstly, the collection of raw EEG signals (containing inter-ictal, ictal, and pre-ictal parts of the EEG signal) using the "RMS Brain View" EEG recording machine has been done at Nilratan Sircar Medical College and Hospital in West Bengal, India. After that, the proposed system performs seizure detection using collected EEG signals. If the system detects any seizure pattern, then a warning message is generated and the system automatically triggers the analytical mode for further analysis. Finally, after completion of the analysis, a detailed report about the upcoming seizure type (generalized/localized), seizure location (lobes), and its likely impacts on the patient has been generated. Figure 1 also represents a function level control flow and data flow design of the proposed system, which has four major steps, namely signal pre-processing, feature collection, segmentation, and post processing result analysis. In the pre-processing state, a raw EEG signal has been recorded and denoised, that make signal ready for execution. After that, the slope and direction of the signal have been changed to encounter the electro-cerebral negativity property of the EEG signal. In the next stage, various features have been extracted from the pre-processed EEG signal. After that, segmentation and nested segmentations have been performed based on those extracted features.

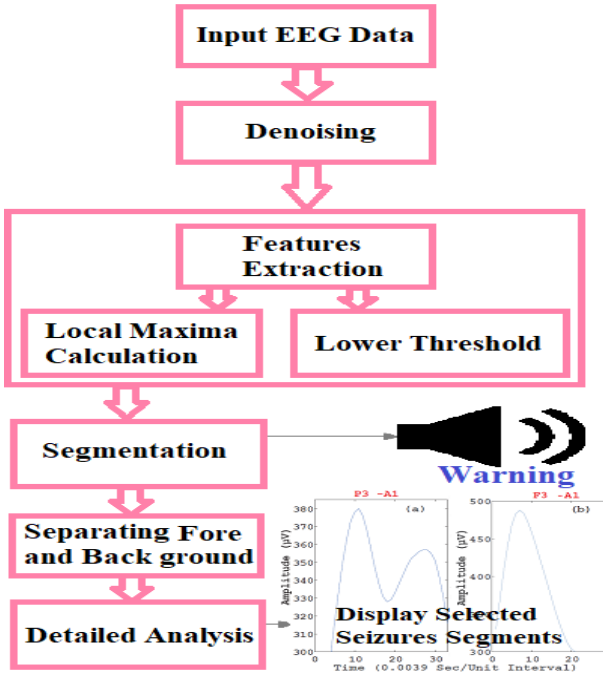

Figure 1. Function-level control flow and data flow of the proposed system

Now these segmented signals were used in analysis, where the abrupt changes in amplitude, power, and energy level of EEG signal segments (spike, foreground, and background) have been detected. With the help of the above features, it can be found that the foreground signal of the spike is different from the background. After that, the seizure's (spike's) field of discharge has been analyzed by using the nearest neighbor method to detect the physiological field of seizure. The epileptic seizure can be identified with location information by the step-by-step execution of the above-mentioned steps.

A detailed working diagram of the proposed system has been given in Figure 2, and descriptions of each and every module have been provided in subsequent part of this section with help of algorithms and suitable images.

2.2. Subject & Dataset Description

In this section, a detail description of the subjects and dataset has been provided. A total of 150 subjects, 65 females and 85 males, with an age group of 18 to 60 years, having an average age of 39 years, are considered for the experiment. Further, the dataset has been classified into two categories: seizure and normal.

Table 1 summarizes the description of subjects, whereas Table 2 summarizes the description of the primary dataset. Here, data have been captured for three sessions with an interval of two weeks between each session, and the duration of each session is 1800 seconds (30 minutes). In the case of 256Hz sampling frequency, a total number of 460.8×10^3 data samples have been recorded in one whole session (1800

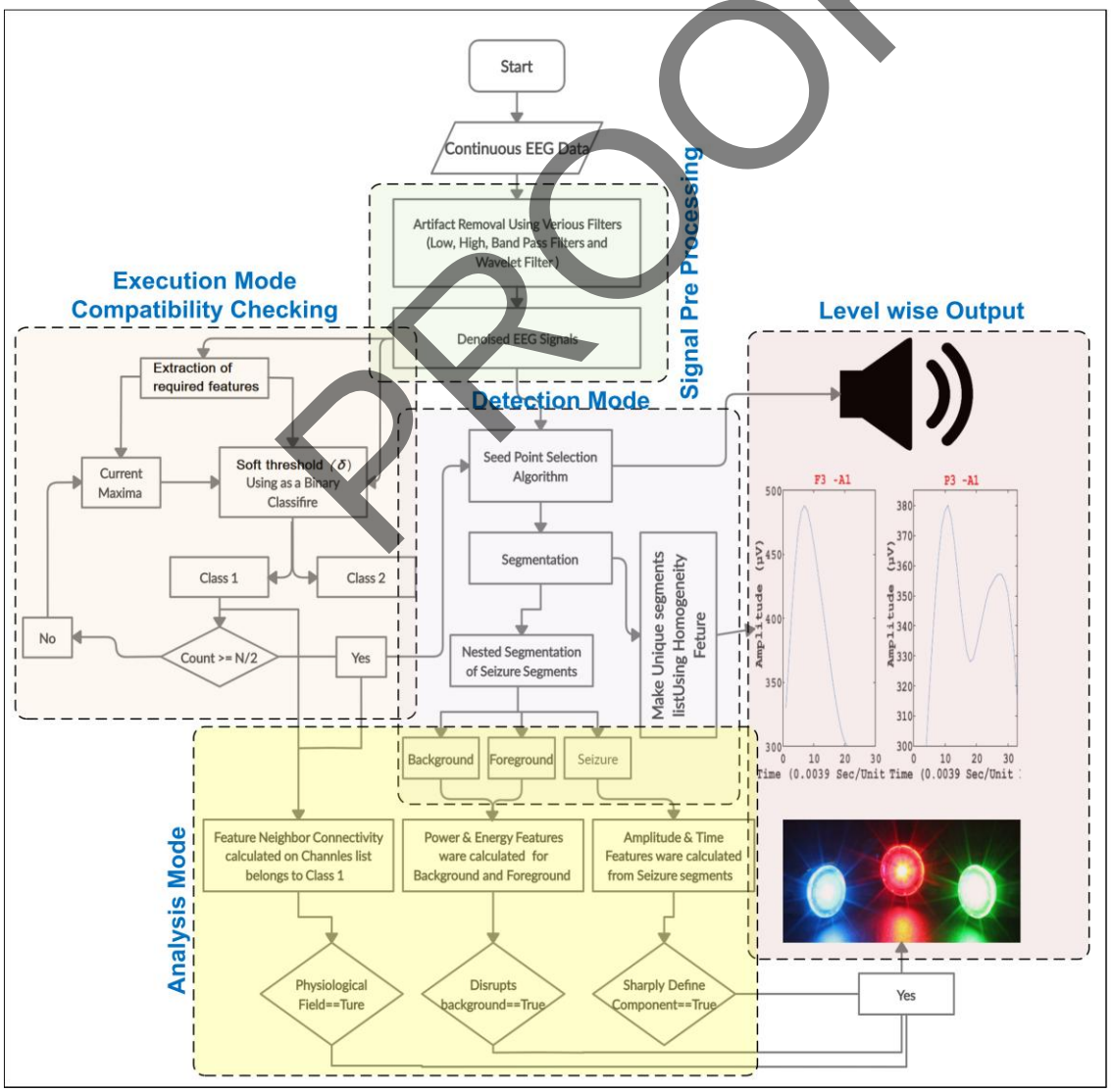

Figure 2. The framework of the proposed system including novel execution mode and analytical mode

seconds) for each patient. For all three sessions, the total duration of the recording is 90 minutes; thus, 1382.4×10^3 samples have been collected for each patient.

Table 1. Subject description

No. Subjects	Age(year)	Gender	Seizure	Normal
85	18-60	Male	67	18
65	18-60	Female	36	29

Table 2. Subject's dataset description (Primary Dataset).

Characteristic	Value
Sampling frequency	256 Hz
Sessions	3
Size of each window	10 sec.
Duration per session	1800 sec.
Per window, the number of data samples	2560
Data samples per session	460.8×10^3
Total duration	5400 Sec.
Total number of data samples per patient	1382.4×10^3

2.3. Data Pre-Processing

This subsection describes signal acquisition and noise removal techniques used in the proposed method.

2.3.1. Signal Acquisition Experimental Setup

Signals were recorded using the RMS Brain View recorder for 30 minutes per session. Here, electrodes are arranged according to the 10-20 system with two different arrangements, called montages. We considered both mono-polar (ear reference) and bipolar montage setups for recording of EEG signal [21, 22]. The monopolar setup is ideal for detecting generalized abnormalities that primarily occur in the central region of the brain. It is often used to eliminate electrocardiograph artifacts from recordings [23]. In this scenario, the ears have minimal influence on brain abnormalities and typically act as a neutral reference point [24, 25]. Furthermore, we have also used a traverse bipolar montage whose derivations are performed from left to right across the head, and channels are usually arranged from front to back. It is useful for the comparison of the left and right hemispheres of brain, and it also provides an easy comparison of the amplitude gradient between the anterior and posterior head. Therefore, it can be said that a bipolar montage setup is good for analyzing low-to-medium-amplitude waveforms [22]. Figure 3 represents both mono-polar and bipolar electrodes placement systems.

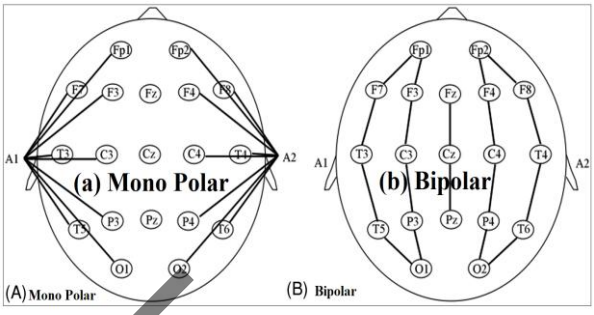

Figure 3. Scalp electrode placement is shown as per the 10-20 system [22, 26]

Filter Setup: The low and high frequency filters have been set at 0.1 Hz and 70 Hz, respectively using a notch filter. The frequency that is greater than 70Hz is trimmed. Further, as per the literature, most of the onset information related to seizure is located in the less than 40Hz frequency range [27, 28]. The High Frequency Oscillations (HFOs) recorded throughout the ictal and inter-ictal phases, which look like the onset seizure pattern (because both have a similar frequency range) [29], so it is very difficult to differentiate seizure wave-form patterns from the HFO pattern. That's why HFOs are being considered pathological and discarded. The major focus of this research is the analysis of the pre-ictal phase of EEG signals. The pre-ictal phase comes before the inter-ictal and ictal phases, which bring the time advantage. Here, the sixteen-channel EEG signals have been acquired and split into 10-second sub-windows for further processing. The length of the above segment is enough to contain more than two (at least three) spikes, related to epileptic seizure of range between 0.07 to 0.3 seconds for each spike [30, 35]. Further, this collectively represents the recursive nature of the epileptic seizure. In Figure 4, a raw EEG signal encompassing all channels has been depicted for reference. These raw signals are used for further processing like noise removal, feature extraction, and classification.

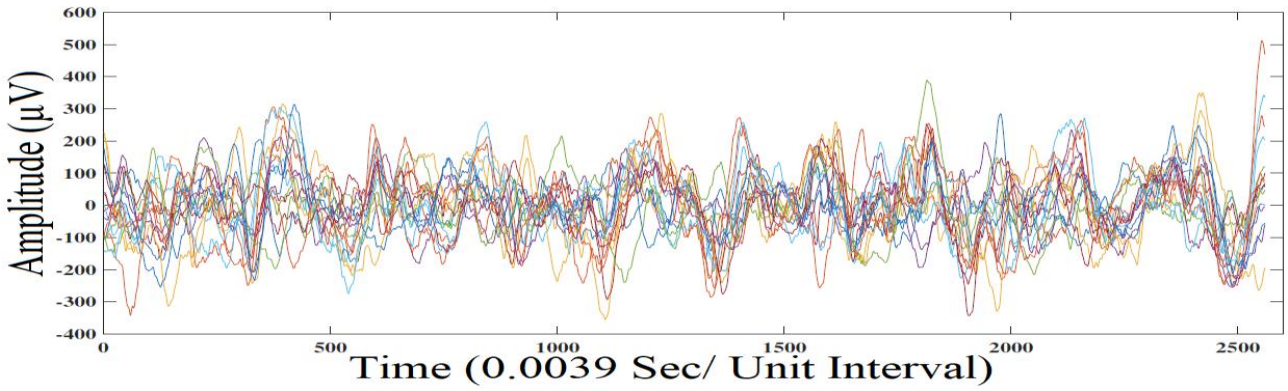

Figure 4. Representation of all 16 channels of EEG signal (10-second), here different colors represent different channels

2.3.2. Noise Removal

After trimming the signal, as mentioned in previous subsection, denoising of the raw EEG signal has been performed. There are several denoising techniques available in the literature, however, wavelet transform-based denoising techniques are prominent and efficient. Das *et al.* (2019) [30] introduced a hybrid technique for noise removal using a modified Haar wavelet, which offers improved speed and memory efficiency. Additionally, in reference [31], a Haar wavelet transform was used to decompose the EEG signal to detect changes in the eye state (from open to closed and vice versa) and to identify visual artifacts in the contaminated EEG signal. Discrete wavelet transform algorithms are preferred for quick results [32–34]. The modified Haar wavelet supports overlapping windows (similar to the Daubechies wavelet), while retaining all the features of the basic Haar wavelet [31, 33]. So, the Haar wavelet has shown better performance than the Daubechies wavelet. In the proposed model, the denoising of the signal is achieved through the utilization of a modified Haar wavelet [35]. In case of modified Haar wavelet transform, divide the incoming signal into even and odd data samples based on the index, SEven and SOdd, where S is an EEG signal and n is the level of denoising. Therefore, Sn can be defined as the union of all even (SEven) and odd (SOdd) data samples at the nth level of denoising. After that, the calculation of the detailed coefficient (S(n, i) Detail) of Haar wavelet transform with a prediction step of the Lifting method by using in-place calculation has been performed ('i' refers to the EEG data sample's index, and n is the level of denoising). Here, the detailed coefficient (S(n, i) Detail) of the ith EEG data sample at the nth level of denoising can be defined as half of the difference between the Sn,(i+1)th and Sn,(i)th EEG data samples. Now calculate the approximation part of the Haar wavelet transform in the update step of the Lifting technique using in-place calculation. First, we calculate the average of two consecutive EEG data samples Sn,(i+1)th and Sn,(i)th, and after that, add half the amount of the detailed coefficient's (S(n, i) Detail) value to the average value. Reiterate the procedure for the continuous incoming EEG signals following the sliding window protocol [35]. The denoising result of a single EEG channel is shown in Figure 5. A raw EEG signal of the F3 lead (channel) has been displayed in Figure 5a, and the corresponding denoising results, as per [30], have been shown in Figure 5b.

2.4. Feature Extraction

In this section, different algorithms used for the extraction of features are described. The proposed work aims to analyze and extract key features from EEG signals and brain structure. This involves identifying sudden shifts in the signal's foreground and background, even when these changes occur at very low amplitudes. Additionally, the study focuses on detecting amplitude deviations, highlighting the electrocerebral negativity nature of the EEG signals, and exploring the formation of physiological fields between multiple electrodes. These features help in understanding the brain's activity and its underlying structure in greater detail, potentially contributing to advancements in neuroscience and clinical applications.

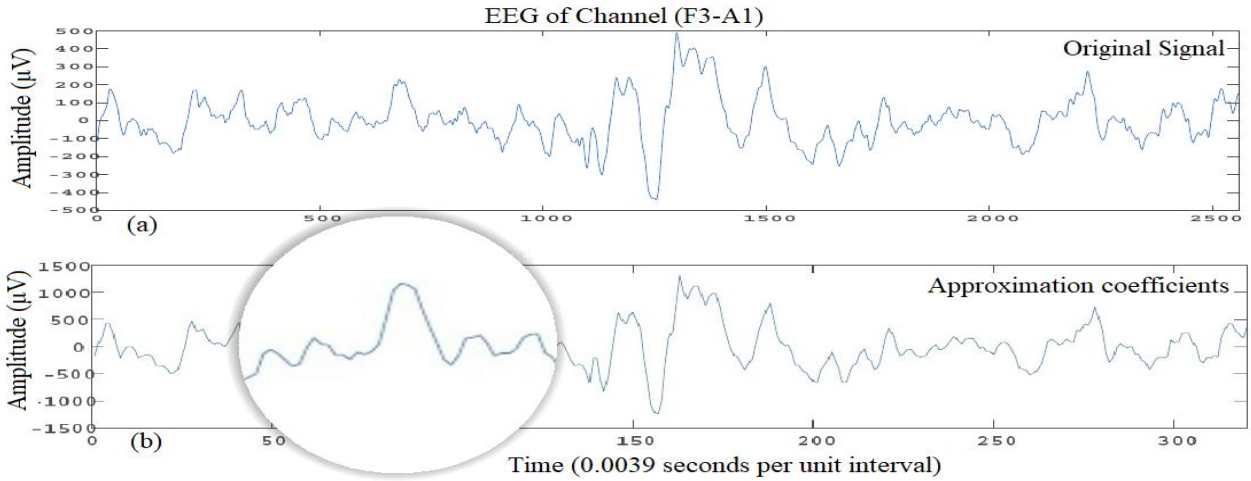

Figure 5. a: showing a raw EEG signal of the F3 lead (channel) of a 10-second window, and b: showing the denoised part of the F3 channel using the modified Haar wavelet-based method

2.4.1. Local Maxima (CL_{max})

The CL_{max} represents the local maximum value (amplitude) of the EEG signal for a specific time window. In Figure 6, the CL_{max} point of channel 1 (FP2- marked by red) and the time stamp of that point have been shown. After that, other channels have also been marked at the same time stamp (index position). Here CL_{max} and (CL_{max} index) define the spike's amplitude and its location in an EEG signal. The detailed calculation of CL_{max} has been given in Algorithm 1, and a conceptual output has been shown in Figure 6.

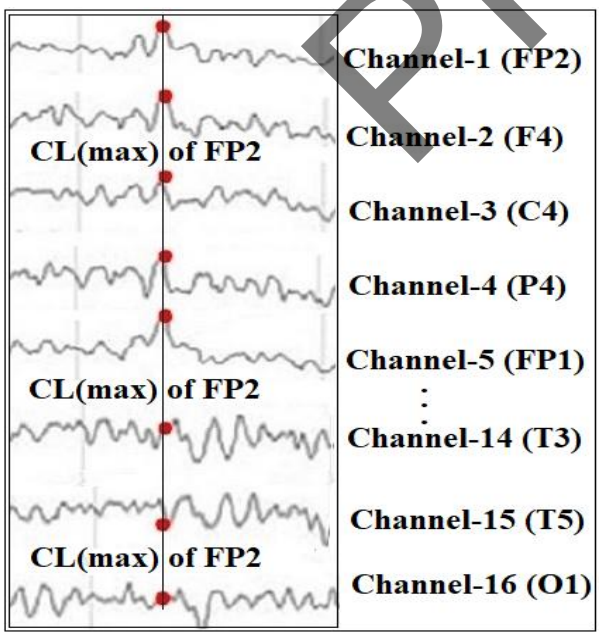

Figure 6. The result of algorithm 1 (local maximum), here the first "red dot" represents the CL_{max} of FP2, and rests of the channels point to the same time indexes of CL_{max}.

Algorithm 1: ***CL**max* calculation

Input: EEG Channel (channel=1)

Output: CL_{max} index

1: $t_{max} \leftarrow$ 10 seconds

2: t ← 1

3: PrevMax ← Assign a large positive value.

4: while (t <= t_{max}) do

5: Calculate the maximum amplitude of an EEG channel at the *t* time index and assign to *CurMax* variable.

6: CL_{max} index ← t

7: if (PrevMax > CurMax) then

8: Use binary classifier function at CL_{max} index point using Eq. (1).

9: PrevMax ← CurMax

10: else if (CurMax => PrevMax) then

11: Update CL_{max} *index* with 0

12: end if

13: Shift the time window *t* by 1 unit interval.

14: end while

15: Repeat Algorithm (1) with the next EEG channel until all CL_{max} for all EEG channels are calculated.

2.4.2. Channel Classification Using Binary Classifier

Here, for channel classification, the soft-threshold value ($\boldsymbol{\delta}$) is used to classify all EEG leads (channels) into two classes (Class 1 and Class 2). The value of soft-threshold ($\boldsymbol{\delta}$) is the average amplitude value of a particular index position (CL_{max}) of the EEG signal, and it may vary for other CL_{max} index positions. Fixed threshold value is not capable of performing equally in all three phases (ictal,inter-ictal, and pre-ictal) of EEG signal, as different signal phases have different ranges of amplitude values. Therefore, soft thresholding is used. Generally, the amplitude value of the ictal phase is greater than the other two phases, and these values are relative values, so soft-thresholding performs better. The value of soft-threshold is calculated by the following Equation 1, and a conceptual output of channel classification for our case has been shown in Figure 7.

$$\boldsymbol{\delta}(\boldsymbol{EEG}\frac{\mathbf{1}}{\boldsymbol{N}}\sum_{\substack{i>=1\\ j=CL_{max}}}^{i<=N\sum}\boldsymbol{EEG}_{[i,j]}\qquad \boldsymbol{CL_{max}} \tag{1}$$

where j = CL_{max} (index) of that channel and i = Channel number.

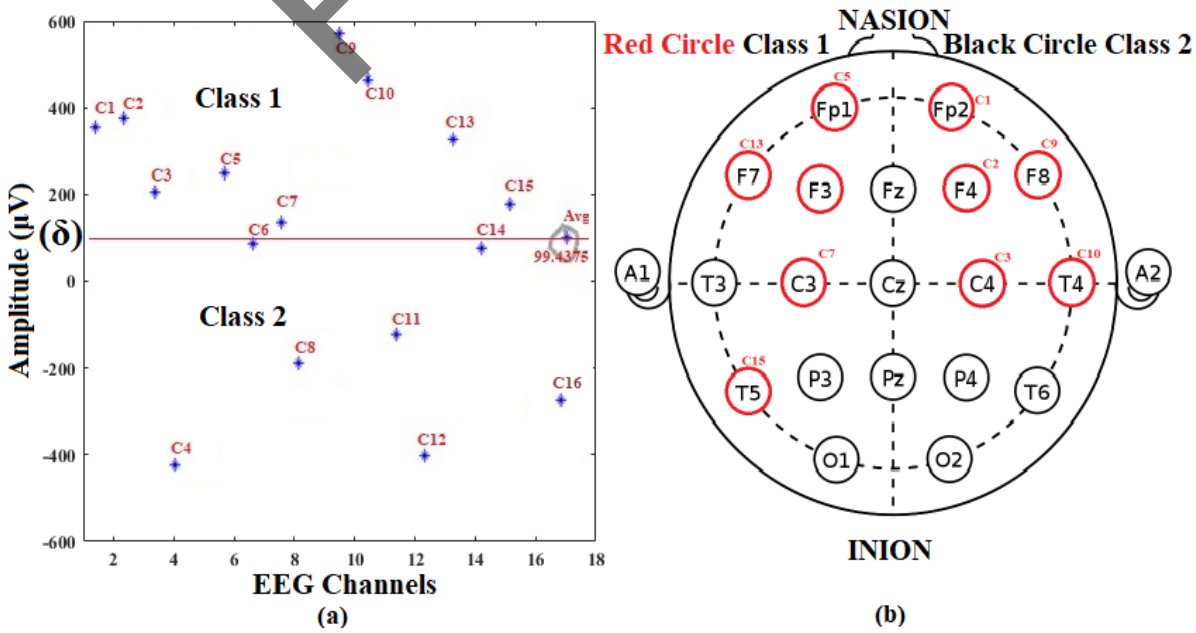

Figure 7. (a) shows a soft-threshold based classification of channels, (b) shows the channels belongs to class-1 only in red

2.4.3. Seed Point Selection

In this section, an algorithm for the selection of seed points in an EEG signal has been described. The seed point refers to an index position of the EEG signals from where a segment begins. For the calculation of the seed point, CL_{max} index position, soft threshold value, and list of channels belonging to class 1 (obtained using Algorithm 1 and 2 and Equation 1) are required. Further, by using Algorithm 2, all channels have been vertically intersected throughout the CL_{max} index position, and each point of intersection is termed as a seed point for the respective segment of EEG channels, which makes EEG signals ready for segmentation. One can understand the concept of seed point selection from Algorithm 2. In this algorithm, a check has been performed between the amplitude of each EEG channel at the CL_{max} index position with a soft threshold value (δ). If the amplitude of that position is greater than or equal to the soft-threshold (δ), then include that EEG channel into class 1 and increase the counter by one. Perform the said task for all EEG channels (N), finally check the value of the count variable, if it is greater than or equal to half of the total number of EEG channels (N/2), then confirm the CL_{max} index position as the seed point.

Algorithm 2: Seed point selection
Input: CL_{max}(index) (from Algorithm 1), Soft Threshold (Eq. 1)
Output: Seed Point Index of all Segments
1: Channels (N) ← Total number of channels
2: SeedList(i,j) ← NULL, (An empty 2D variable where j= time index and i=channel)
3: Class1 ← NULL, (1D empty array.)
4: for (Channel i=1 to N) do
5: count ← 0
6: j ← CL_{max}(index)
7: Avg value ← Soft threshold Value
8: if the amplitude of EEG channel *i* at *j* time index is greater than Avg value (Soft threshold), then
9: count ← count+1
10: Add EEG channel "i" into Class1 array
11: end if
12: end for
13: if (count >= n/2) then
14: Seed point ← True
15: Store the *j* time index of the *i* EEG channel into the Seed List variable.
16: Create segments using seed point indexes with the help of equation (2).
17: else
18: Make seed point false at *j* time index of *i* EEG channel.
19: Call Algorithm-1 for the next CL_{max} (index) calculation.
20: end if

2.4.4. Segmentation

Here, as per Equation 2, the use of a dynamic approach to calculate the length of the signal segments gives a special edge to the proposed algorithm over existing state-of-the-art. It also provides flexibility to cover a large number of databases with various frequencies of EEG signals. For the segmentation of the signal, Equation 2 will be used, which is given below:

$$\boldsymbol{\Delta(EEG_{[i,j]}) = \left(EEG_{(i,(spi-(\frac{sl}{2}))} \rightarrow EEG_{(i,(spi+(\frac{sl}{2}))}\right)} \quad (2)$$

where *i* denotes the channel, *spi* denotes the seed point index, and *sl* denotes the segment length, respectively.

Segment ($\Delta_{(i,\,j)}$) is obtained from the j^{th} seed point of the i^{th} channel of signals, where i = 1, 2, 3...N; and j = 1, 2, 3, ...S. Here, N refers to the number of channels, and S refers to the total number of possible seed points. Further, a bidirectional walk has been performed from the seed point location (*spi*) to (*−(sl/2)*) and (*+(sl/2)*) locations for all possible seed points. All segments of every possible seed point of the given signal have been shown in Figure 8.

2.4.5. Heterogeneous Segment Selection

After the segmentation, heterogeneous segments are selected based on feature similarity. In this method, an EEG signal segment has been considered and compared with others. Further, if a match is found between any two segments, then one of them is removed. This process continues until all duplicate segments associated with class-1 are eliminated from all channels. The above task will be performed using the following Equation 3:

$$\Delta(EEG_{[i,j]}) = \begin{cases} Drop\Delta(EEG_{[i,j]}), & if \quad \Delta(EEG_{[p,q]}) = \Delta(EEG_{[i,j]}) \quad when \quad (j \neq q) \wedge (i \neq p) \\ \text{continue}, & \text{otherwise} \end{cases} \quad (3)$$

2.4.6. Physiological Field Detection

Physiological field detection depends on the geographical features of the human brain. The logical zonalization of the brain is called a lobe. The EEG channels are named according to the lobes where they are placed on the scalp. Two or more directly connected lobes (domains) create a physiological field, which is one of the necessary criteria for epileptic seizure classification (focal or general seizure), as shown in Figure 9. A list of channels belonging to a set of domains (lobes), where an epileptic seizure was experienced, can be identified by the Algorithm 3. Further, the connected domains (nearest neighbor lobes) are being shortlisted from the set of domains having seizure using the domain connectivity matrix. To show the conceptual output of this algorithm, we marked all nearest neighbor lobes in red and green colors as shown in Figure 9. From Figure 9, it is clear that the fields have been formed by directly connected frontal lobe (channel F4) and central lobe (channel C4) and front-o-parietal lobes from different hemispheres (channels FP1, FP2), which are marked by red and green colors, respectively. Algorithm 3 describes the process of physiological field detection in detail, where the term "field" is referred as physiological field of the brain.

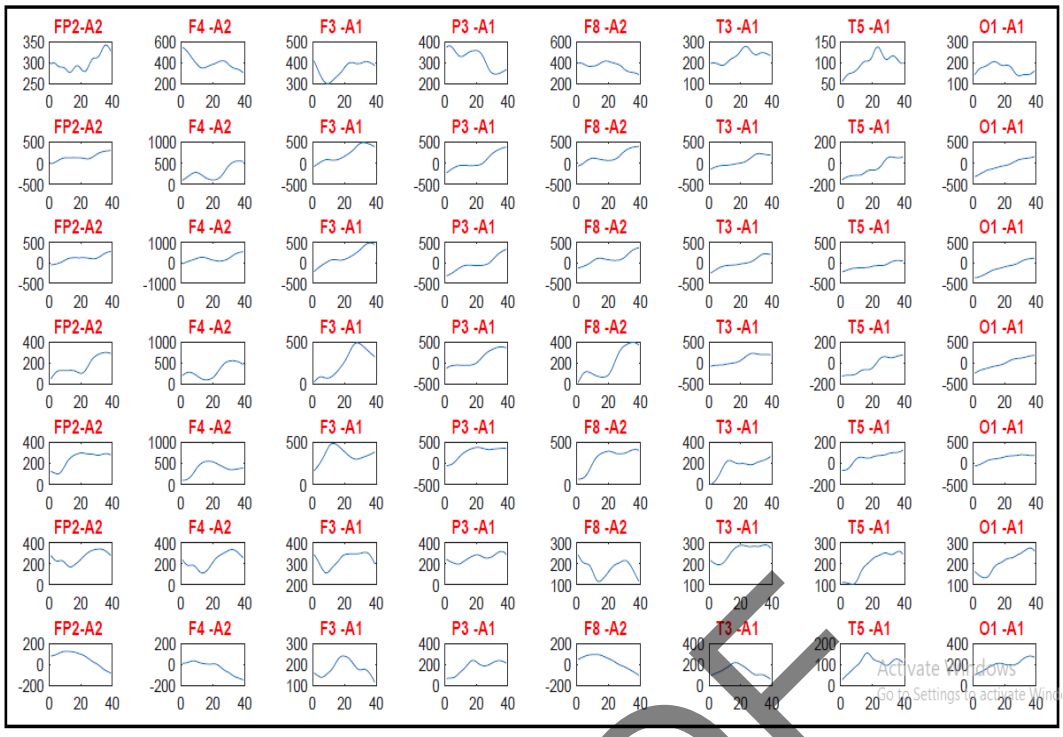

Figure 8. Showing all possible segments obtained from the segmentation process. Here, the columns represent the channels belonging to class 1 only, and each row represents all different seed points

Algorithm 3: Physiological Field Detection
Input: Class1 Channel List from Algo. (2) And EEG Segment from Equation 3.
Output: Field List of EEG channels having field features.
1: Domain Connectivity Matrix (DC[i,j])

$$DC_{[i,j]} \leftarrow \begin{cases} 1, & \text{if Domain(i) is connected to Domain(j)} \\ 0, & \text{otherwise, here i and j boths are channels} \end{cases}$$

2: A 2D matrix is used to store all *Segment [i,t]*, where *i* represents the channel and *t* represents the time index of that channel.
3: An empty 1D array *FieldList[]* is taken to store the final channel's list.
4: Count the number of channels belonging to *class 1* and store into *n* variable.
5: for (j = 1 to n) do
6: Select a channel *j* from *Class1* Channel List and store it into variable *ChRef*
7: Add *ChRef* channel into Field List
8: for (i = 1 to n) do
9: Add the rest of the channels belonging to *Class1* into a 1D array *ChRest.*
10: if ((DC[ChRef,ChRest]= =1) && (ChRef != ChRest)) then
11: Add *ChRef* into Field List if *ChRef* and *ChRest* have a direct connection except for self-loop connection.
12: end if
13: end for
14: Make Field List Distinct
15: j ← j+1
16: end for
17: Finally, return the Field List array containing a list of EEG channels having a physiological field feature.

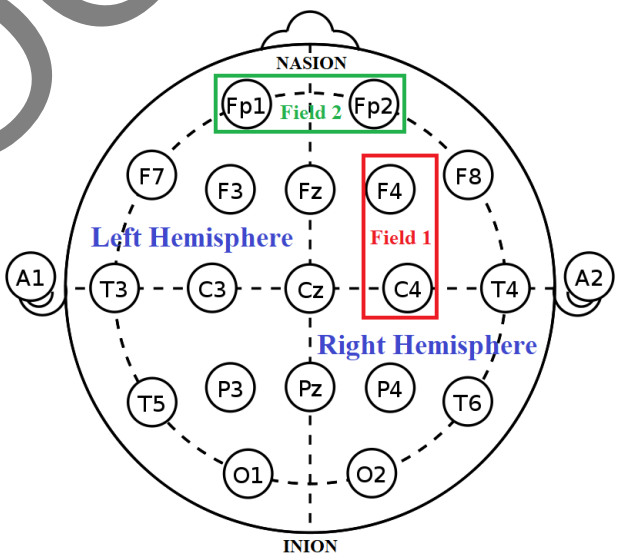

Figure 9. The algorithm's result shows red and green boxes representing connected channels between different (central and frontal) or the same (fronto-parietal but from different hemispheres) brain lobes

2.4.7. Background Analysis of Tentative Seizure

After obtaining all segments as a result of Equation 3, the segments were subdivided into spike, background, and foreground for further processing. The division process involves confidently identifying

the spike within the segment and then decisively splitting the EEG signal into its background and foreground parts. After that, the energy and power of those parts are computed using Equations 4 and 5. The power of the signal is defined as:

$$P_t \equiv \lim_{\substack{i\to\infty \\ j\to\infty}} \left(\frac{1}{t_i + t_j + 1} \sum_{t=t_i}^{t_j} E_t \right) \quad (4)$$

The energy of foreground, background, and spike of signal segments, represented by E_t, is calculated by the following Equation 5:

$$E_t \equiv \sum_{t=t_i}^{t_j} |f(t)|^2 \quad (5)$$

where t_i and t_j represent the starting and ending points of the segment of EEG signals, and $f(t)$ is the frequency of a particular time instance t.

The background signal is considered from t1 to t2, while the spike and foreground signals are considered from t2 to t3 and from t3 to t4, respectively. Here, temporary changes in power and energy level of foreground and background signals have been detected with the help of Equations 4 and 5. It indicates that the proposed method can successfully identify the necessary property of epileptic seizure in the presence of a disturbing background. In Figure 10, a typical epileptic seizure segment with all three sub-sections has been shown. From Figure 10, it is clearly visualized that the foreground signal (from t3 to t4) is completely dissimilar to the background signal (from t1 to t2) after the occurrence of the epileptic seizure spike signal (t2 to t3).

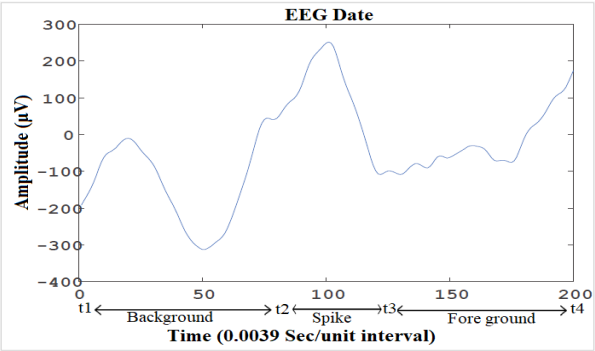

Figure 10. A particular EEG signal's segment and its sub-segments: spike, background & foreground

3. Results and Discussion

The study has been carried out using Matlab (R2017b, 64-bit) on a Windows 10 (64-bit, Intel Core i7, 8GB RAM). A primary dataset comprising 150 subjects obtained from Nilratan Sircar Medical College and Hospital in West Bengal, India, was utilized. For more information about the experimental subjects and the dataset, refer to Tables 1 and 2 in section 2.1. The subsequent sections present a comprehensive analysis of output patterns, time, and performance.

3.1. Output Analysis

The following section presents the results obtained from various subjects and analyzes these outputs based on their EEG signal patterns (spike, spike-wave, etc.). The method proposed in the study accurately detected 102 out of 150 seizure patients with a true positive rate of 91.07%. The output results underwent verification and approval by several medical practitioners and neurology experts. In Table 3, the decisions made by the proposed algorithm for the first 12 subjects out of 150, along with their corresponding ground truth results, are displayed. For simplicity, the detailed output of three randomly selected patients out of the 102 seizure-affected patients has been analyzed, and various output patterns have been shown. Specific segments corresponding to each channel have been identified through background analysis for potential seizure, considering power and energy features. A referential montage setup (monopolar) was used for subjects 1 and 2, while a bipolar montage setup was used for subject 3. The suspected segments of subjects 1, 2, and 3 are visually represented in Figures 12, 13, and 14, respectively. It was determined that out of the sixteen input channels, only eight channels (FP2, F4, F3, P3, F8, T3, T5, O1) are likely affected by epileptic seizures for both subject 1 & subject 2.

For adding a more detailed description of the subjects (1, 2, and 3), here we perform a zoom-in operation on the segments that contain suspected epileptic seizure waveforms. Each of these segments is associated with specific waveform patterns, such as "spike" and "spike & wave," which confirm the distinct characteristics of epileptic seizures and complex seizure waveforms. Furthermore, some

Table 3. Shows the results of the proposed method with ground truth for the primary dataset

S.No.	Name	Sex	Onset Seizure	Epilepsy	Ground Truth (Report)	Proposed System Report
1	Subject-1	M	No	Yes	Positive	Positive
2	Subject-2	M	No	Yes	Positive	Positive
3	Subject-3	M	No	Yes	Positive	Positive
4	Subject-4	F	No	Yes	Positive	Positive
5	Subject-5	M	No	Yes	Positive	Positive
6	Subject-6	F	No	Yes	Positive	Positive
7	Subject-7	F	No	No	Negative	Positive
8	Subject-8	F	No	No	Negative	Negative
9	Subject-9	M	No	Yes	Positive	Positive
10	Subject-10	F	No	Yes	Positive	Positive
11	Subject-11	M	No	Yes	Positive	Positive
12	Subject-12	M	No	Yes	Positive	Positive

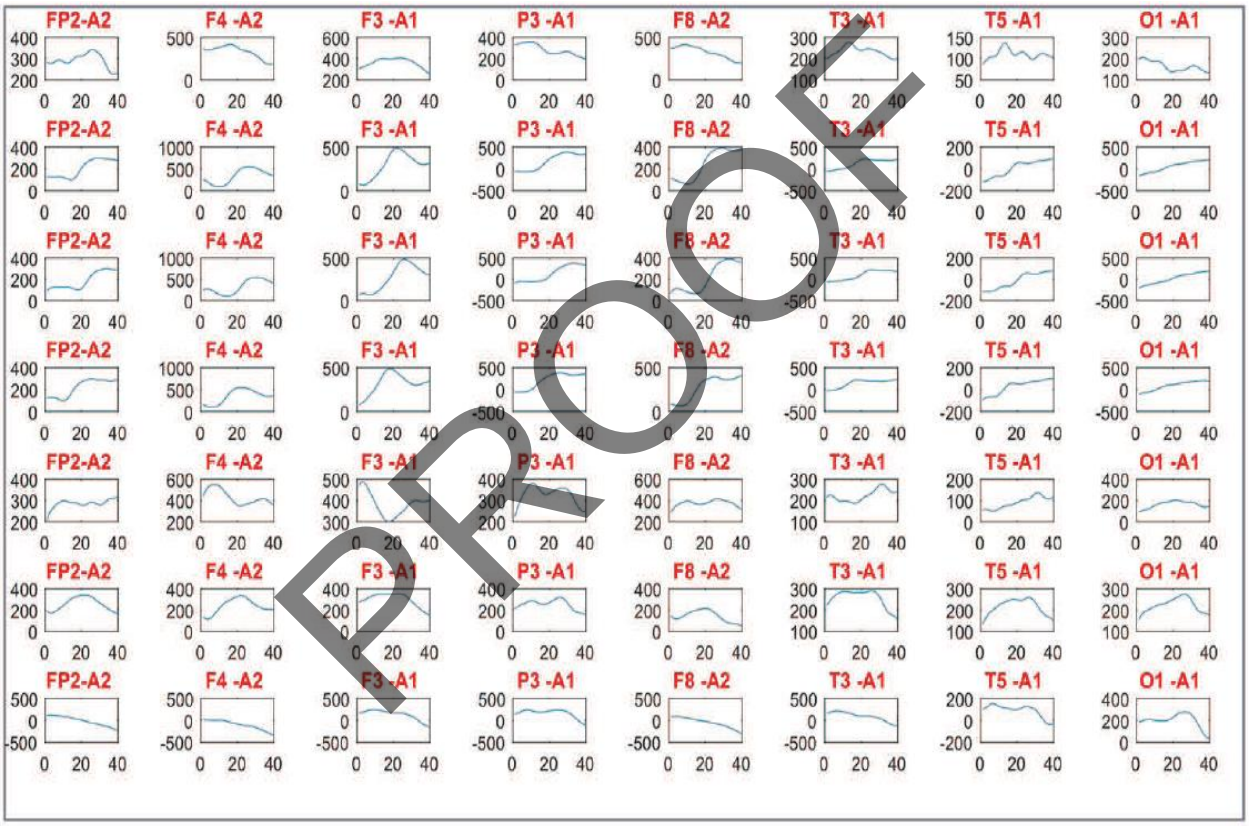

Figure 11. Subject 1: Output of suspected segments with channels containing epileptic seizure wave-forms. The method predicts eight channels (highlighted in red) where a seizure may occur. X-axis represents "Time (0.0039 seconds per unit interval)," and the Y-axis represents "Amplitude (μV)."

segments are selected from subjects 1 and 2, and their zoomed versions are shown in Figures 14 and 15. Here, a spike waveform has been selected from the F3-A1 channel (4th row and 3rd column of Figure 11 representing subject 1) and shown in its zoomed version in Figure 14a. Further, a spike & wave pattern has been selected from the P3-A1 channel (5th row and 4th column of Figure 12 representing subject 2) and shown as a zoomed version of that in Figure 14b.

Also, some different waveform patterns, like thick and thin spikes have also been shown in Figure 15 obtained from Figure 13 (subject 3). From both Figures 14 and 15, it is clearly visible that the spike amplitude values in Figure 14 are higher than those in Figure 15.

Based on this observation, it can conclude that the proposed method operates efficiently for both high and low amplitude values. Further the top labels of Figures 14 and 15 clearly indicate the seizure spike's

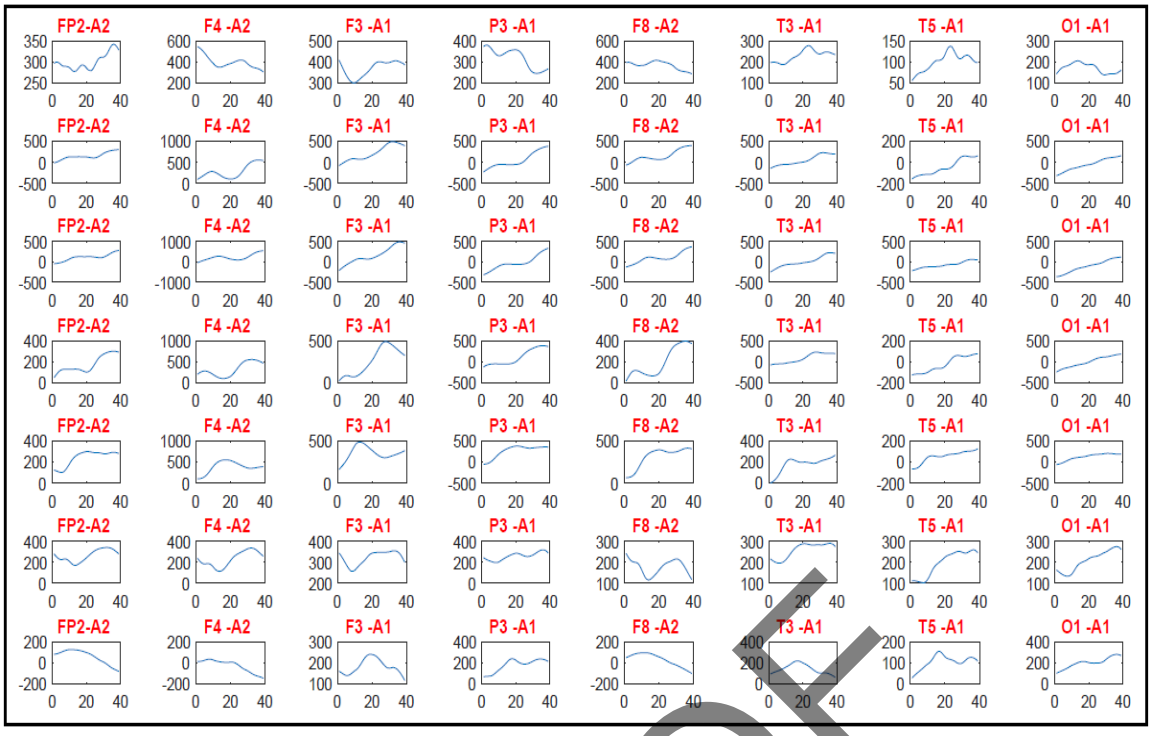

Figure 12. Subject 2: Output of segments with channels containing epileptic seizure waveform. This method identifies eight channels (highlighted in red) where a seizure may occur. X-axis represents "Time (0.0039 seconds per unit interval)," and the Y-axis represents "Amplitude (μV)."

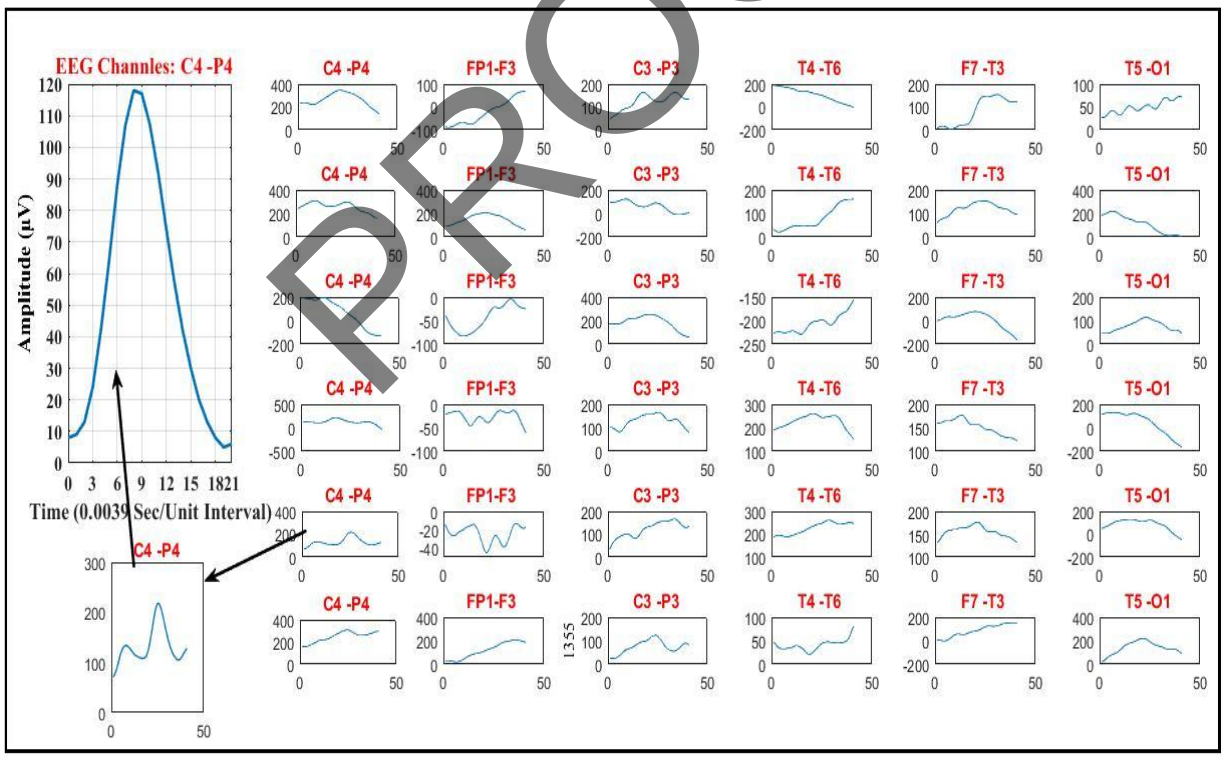

Figure 13. Zoomed spike waveform related to epileptic seizure, taken from the channel C4-P4 (5th row, 1st column)

location (F3, P3, C4-P4) and montage information (Mono-polar montage: F3-A1, Bipolar montage: C4-P4). Based on the seizure spike's location, the study suggests that predictions can be made about the patient's upcoming condition. Furthermore, the y-axis of Figure 15 shows two values in blue, representing the time index of the seizure spikes. This clearly indicates that the patient experiences multiple seizures, referred to as recurring seizures.

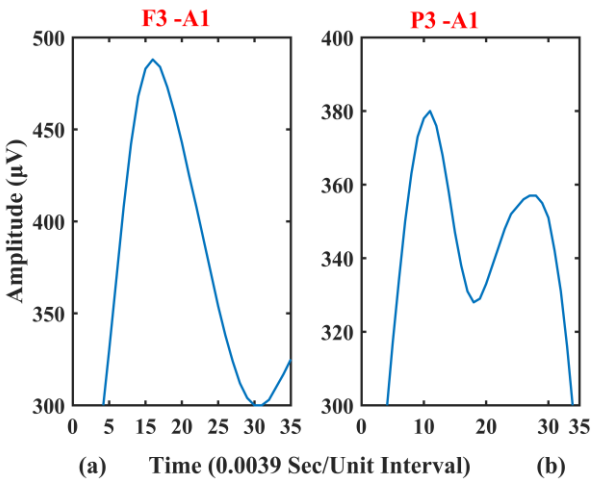

Figure 14. Shown epileptic seizure waveforms: Here, the sub-figure (a) expanded spike & wave pattern from the channel P3-A1 (5th row, 4th column of Subject 2), and another sub-figure (b) expanded spike waveform from the channel F3-A1 (4th row, 3rd column of Subject 1)

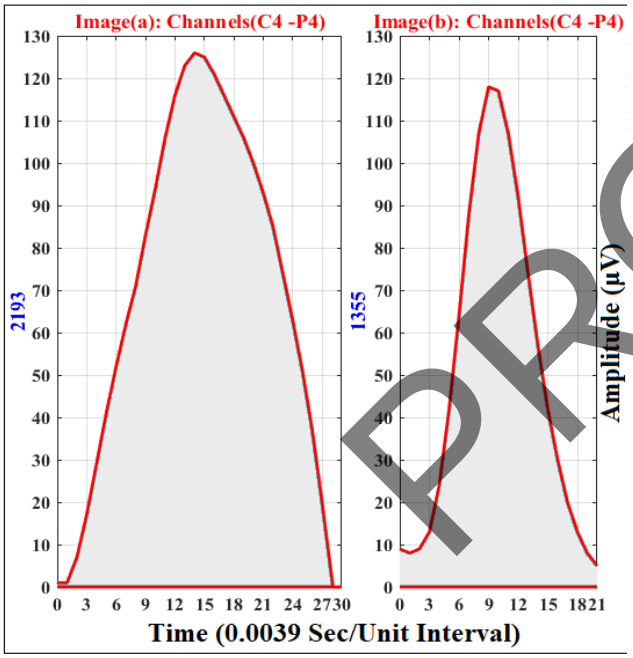

Figure 15. Shown the epileptic seizure waveforms: Here the sub-figure (a) showing the expanded version of the waveform pattern thick spike which is getting from the channel C3-P4 (1st row, 1st column of Figure 13), and sub-figure (b) shows the expanded EEG pattern of thin spike obtained from the channel C3-P4 (5th row, 1st column of Subject 3

3.2. Time Analysis of Predicted Seizure

The proposed method operates in two modes: detection and analysis. The advance prediction time is calculated when the actual seizure occurrence time is known. The actual seizure occurrence time (Tact) is 5 seconds before the real-time recording (Tr). Since there are two different modes of execution, the execution time is considered separately for detection (Td) and analysis (Ta). The advance prediction time (Tadv) for the detection mode is calculated by subtracting the execution time for detection (Td) from the actual seizure occurrence time (Tact). The advance prediction time (Tadv) for the analysis mode is calculated by subtracting the cumulative execution time for detection (Td) and analysis (Ta) from the actual seizure occurrence time (Tact).

The analysis results of the proposed methodology can be found in Table 4. The "EEG File" column represents each patient, and the "Time Window" column indicates fixed 10-second intervals. It's worth noting that starting from window-5 of patient-1, the proposed method demonstrated its ability to detect seizures 52.59 seconds in advance and prepare analytical reports 38.04 seconds before the seizure occurrence. For patients 2 and 3, the "X" symbol indicates that seizure detection is confirmed, but the analysis report does not justify the detection result. For patient 4, the methodology successfully identified seizure occurrences 52.69 seconds in advance and produced analytical reports 43.177 seconds ahead of the seizure.

In summary, the proposed method can predict epileptic seizures in advance of their actual occurrence time. By utilizing the pre-ictal part of EEG, the method detects epileptic seizures before the onset of the seizure phase, allowing for advanced prediction.

3.3. Performance Analysis

In order to demonstrate the effectiveness of the proposed method, various performance measurement parameters such as precision, recall/sensitivity, specificity, prevalence, accuracy, and F1 score were utilized. The confusion matrix represented the positive and negative classes as seizure and normal cases, shown in Figure 16. The performance parameters and results of the proposed system are provided in Table 5. The precision (99.00%) and recall scores (91.07%) were calculated using Equation 6 and Equation 7, respectively. Furthermore, the specificity (97.36%) indicates the ratio between predicted negative observations and actual negative observations, while the prevalence score (74.66%) refers to the number of

Table 4. Performs detection and prediction time analysis of our proposed model using the primary dataset

EEG File	Time Window Before Seizure (T_r)	Actual seizure time (T_{act}) time in seconds	Execution time based on execution mode in seconds		Advanced prediction in seconds (T_{adv})	
		$T_{act} = (T_r+5)$	Detection (T_d)	Analysis (T_a)	T_{adv} (D)	T_{adv} (A)
Patient-1 (Window 1)	1-10	15	2.54	16.02	12.46	-1.02
Patient-1 (Window 2)	11-20	25	2.30	15.16	22.70	9.86
Patient-1 (Window 3)	21-30	35	2.65	30.55	32.35	4.45
Patient-1 (Window 4)	31-40	45	2.56	10.13	42.44	34.87
Patient-1 (Window 5)	41-50	55	2.41	16.96	52.59	38.04
Patient-2 (Window 1)	1-10	15	2.55	x	12.45	x
Patient-3 (Window 1)	1-10	15	2.66	x	12.34	x
Patient-3 (Window 2)	11-20	25	2.42	x	22.58	x
Patient-3 (Window 3)	21-30	25	2.17	x	22.83	x
Patient-4 (Window 1) (True -ve)	1-10	15	x	x	x	x
Patient-4 (Window 2)	11-20	25	2.54	36.23	22.46	-11.23
Patient-4 (Window 3)	21-30	35	2.23	69.38	32.77	-34.38
Patient-4 (Window 4)	31-40	45	2.59	12.79	42.41	32.21
Patient-4 (Window 5)	41-50	55	2.31	11.83	52.69	43.177

observations that belong to the positive class among the total observations. The accuracy of 92.66% shows the total number of correctly predicted observations by the proposed system, signifying a significantly good result. The F1 score, which is 94.86%, demonstrates that the proposed method performs well even in the case of an imbalanced dataset. Further, it represents the weighted average of precision and recall scores and has been calculated using Equation 8. For a more detailed and in-depth analysis of the result, here the 95% CI (confidence interval) has been calculated for each and every statistical parameter provided in Table 5. Further, the Mc-Nemar test has been performed, which gives an exact p-value of 0.0117 (1.17%), indicates that the result is statistically significant and strongly rejects the null hypothesis.

$$Precision = \frac{TruePositive}{(TruePositive + FalsePositive)} \quad (6)$$

$$Recall = \frac{TruePositive}{TruePositive + FalseNegative} \quad (7)$$

$$Recall = \frac{TruePositive}{TruePositive + FalseNegative} \quad (8)$$

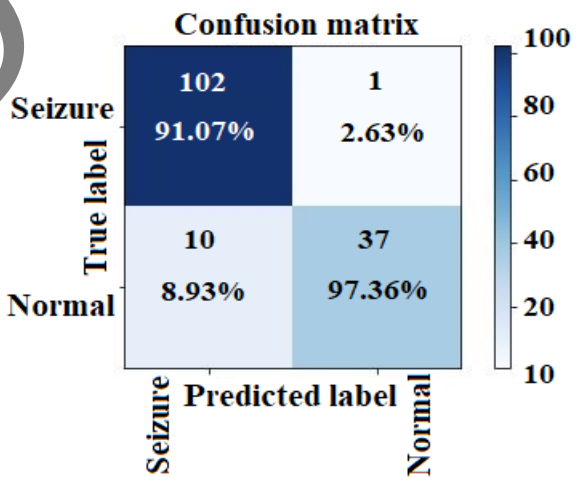

Figure 16. Confusion matrix based on the result of the primary dataset obtained by the proposed system

Table 5. Performance matrix and various other statistical measures of the primary dataset have been provided below

Parameters	Score (%)	95% CI
Precision	99.02	93.64% to 99.86%
Recall	91.07	84.19% to 95.64%
Specificity	97.36	86.19% to 99.93%
Prevalence	74.66	66.93% to 81.41%
Accuracy	92.66	87.25% to 96.28%
F1 Score	94.86	91.36% to 98.41%
Exact P-value (Mc-Nemar test)	0.0117 (1.17%)	01.77% to 10.23%

3.4. Comparison

The proposed method has also been tested on a secondary data set available open source. The data set of this secondary dataset#1 has been collected from Sir Ganga Ram Hospital by an IIT-Delhi research group [37]. The said group thoroughly worked on this data set using several methods and features, and published their findings in [38- 40], as shown in Table 6.

As per the reported results, Probabilistic Neural Network (PNN) and Discrete Wavelet Transform (DWT) based models require 45 features to achieve the best accuracy (100%) [38]. Further, the secondary dataset#2 has also available open source published by S. Panwar *et al.* in 2020 [41]. Our proposed method successfully achieved the same using only 8 features and also outperforms other methods in terms of accuracy, sensitivity, and specificity. Further, the secondary dataset#2 is also available open-source data set published by S. Panwar *et al.* in 2020 [41]. Our proposed method successfully achieved better results using only 8 features and outperformed other methods in terms of accuracy, sensitivity, and specificity. As shown in Table 6, it is clear that the proposed method provides the best and most optimal solution compared to the other methods. Furthermore, the secondary dataset#3 is also known as the CHB-MIT scalp EEG dataset, which is a freely available open-source dataset published by A.L. Goldberger *et al.* in 2000 [45]. Our proposed method successfully outperformed other state-of-the-art methods in terms of accuracy, sensitivity, and specificity with detection mode and also showed a promising result in combined mode execution (detection and analysis mode). As shown in Table 6, it is clear that the proposed method provides the best and most optimal solution compared to the other methods.

The proposed automated system for epileptic seizure prediction utilizes various advanced and fundamental features related to time, location, frequency, and

Table 6. Comparison of the proposed model with state-of-the-art methods, based on the several secondary datasets

Work	Method + Features	Accuracy	Sensitivity	Specificity	Features
Comparison with Secondary Dataset #1 [37]					
Gandhi *et al.* (2010) [38]	PNN+DWT+EDA	99.33%	99.60%	99.00%	1
T. Gandhi *et al.* (2010) [38]	PNN+DWT+STD	97.90%	98.20%	97.60%	1
T. Gandhi *et al.* (2011) [39]	PNN+Energy+Wavelet(Coif1)	99.35%	-	-	1
T. Gandhi *et al.* (2011) [39]	SVM+Energy+Wavelet(Coif1)	96.11%	-	-	1
T. K. Gandhi *et al.* (2012) [40]	PNN+ DWT+ Several Features	100.00%	100.00%	100.00%	45
Swami *et al.* (2016) [41]	PNN+ DWT	100.00%	100.00%	100.00%	-
K. Das *et al.* (2020) [42]	Basic Mode+statistical features	92.66%	91.07%	97.37%	7
Proposed	**Proposed**	**100.00%**	**100.00%**	**100.00%**	**8**
Comparison with Secondary Dataset #2 [43]					
S. Panwar *et al.* (2019) [44]	Retrained Model + LBP	69.00%	-	-	-
S. Panwar *et al.* (2019) [44]	Retrained Model + TF	73.00%	-	-	-
Proposed	**Proposed**	**96.00%**	**97.95%**	**88.55%**	**8**
Comparison Secondary Dataset #3 [45] (CHB-MIT scalp EEG dataset of 22 Patients)					
Cho *et al.*, (2016) [46]	SVM+ MEMD	87.70	82.80	83.00	-
Khan *et al.* (2018) [47]	CNN+ Wavelets	86.60	87.80	85.30	-
J Hellar *et al.*, (2022) [48]	SVM+ EmDMD	89.30	90.10	88.50	-
J Hellar *et al.*, (2022) [48]	RF+ EmDMD	91.30	92.80	89.70	-
C. Li *et al.*, (2023) [49]	FB-CapsNet	89.60	-	-	-
Shah *et al.* (2024) [50]	-	93.27	90.1	96.53	-
Kunekar P., *et al.*, (2024) [51]	-	97.1%	95.00	-	-
T. Shawly *et al.*, (2005) [52]	LHAENA	98.00	96.71	96.67	-
Proposed	**Proposed (Detection Mode)**	**100.00%**	**100.00%**	**100.00%**	**8**
Proposed	**Proposed (Detection+ Analysis)**	**96.00%**	**97.95%**	**88.55%**	**8**

[**Note:** LBP: Local Binary Pattern, TF: Time-Frequency, MEMD: multi-variant empirical mode decomposition, RF: random forest, EmDMD: embedded dynamic mode decomposition**,** LHAENA: lightweight hybrid attention ensemble network architecture.]

statistical metrics to outperform existing state-of-the-art methods. For instance, this system makes use of low-amplitude deviation and rhythmic irregularities to identify a wide range of epileptic seizures from all parts of the EEG signal. Additionally, the model extracts location features from EEG channels and analyzes brain structure (spatial features) to detect both local and generalized seizures. Moreover, it incorporates various statistical features, including energy, power, and cross-correlation of EEG signals, to analyze sudden changes in both the foreground and background of the signal. This allows the detection of slight amplitude deviations in EEG signals, even at low levels, enabling the model to identify seizures across different frequency bands and a wide spectrum of amplitude values. Furthermore, the study emphasizes the electro-cerebral negativity feature and the physiological fields between multiple electrodes, which help to reduce false positives and enhance the model's accuracy. This combination of features empowers the proposed model to outperform various existing models in the field.

4. Conclusion

In the modern era, the increasing number of EEG leads in EEG machines poses a significant challenge in continuously monitoring and promptly identifying specific seizure areas. To tackle this issue, a robust classification technique has been proposed to distinguish EEG signals into two categories: normal and epileptic seizure discharge. The proposed system confidently predicts seizures from the pre-ictal phase of the EEG signal, providing a clear time advantage over other methods. A set of algorithms reliably identifies all such seizures located inside all channels, which may not be visible through visual interpretation. Additionally, the proposed method accurately identifies waveforms indicating a likely seizure and confidently predicts upcoming epileptic seizures. Furthermore, considering the physiological field properties, this system confidently generates a detailed report about seizure type (generalized/localized), seizure location (lobes), and potential impacts on patients in advance. After witnessing a seizure in advance, the proposed system generates an alarm to alert neurologists and assist them in locating seizures and saving precious human lives. A test was conducted here on the 150 subjects (Primary Dataset), and we achieved significantly good results. The proposed system performs satisfactorily with an accuracy of 92.66% and an F1 score of 94.86% for predicting seizures from the pre-ictal phase of the EEG signal. We also tested the proposed method on a secondary dataset [37] and successfully achieved good results using very few numbers of features. In EEG signals, the pre-ictal phase follows the ictal phase (seizure onset). Therefore, the proposed system predicts epileptic seizures in advance and provides probable location information for upcoming seizures. This advancement could lead to substantial improvements in the field of neuroscience.

The novelty of the proposed automated system for epileptic seizure prediction lies in its multidimensional and integrative feature extraction methodology, which significantly advances beyond existing state-of-the-art approaches. The system leverages a diverse set of features encompassing temporal, spatial, frequency-domain, and statistical characteristics of EEG signals to enhance predictive performance. Specifically, it utilizes low-amplitude deviations and rhythmic irregularities across the full EEG signal to accurately identify a wide range of seizure types. Spatial features are extracted by analyzing the anatomical distribution of EEG channels and underlying brain structures, enabling effective detection of both focal and generalized seizures. Furthermore, the model incorporates statistical descriptors such as signal energy, power, and cross-correlation to capture abrupt signal transitions in both the foreground and background, including low-amplitude variations across multiple frequency bands. The inclusion of electro-cerebral negativity and inter-electrode physiological field features contributes to a substantial reduction in false positives, thereby improving the overall reliability and accuracy of seizure prediction. This comprehensive feature integration framework constitutes the primary contribution of the proposed work and demonstrates clear superiority over conventional models in the field.

However, the proposed model (algorithms) has been implemented here using LAN-based systems, which present challenges related to LAN networks. To overcome this, the system needs to be more compact. A Body Area Network (BAN) could be one solution. Furthermore, the studied system has a missing electrode issue, which can be resolved by using a BCI

(Brain-Computer Interface) or an Emotive-type head-mounted EEG sensor, which also offers compactness. Therefore, we plan to develop a novel, compact, and portable device in the near future. This device will effectively address the missing electrode problem in real time and be easily transported and used in diverse environments.

Acknowledgment

We would like to express our sincere gratitude to Nil Ratan Sircar Medical College and Hospital, Kolkata, India, for granting access to the dataset necessary for conducting our research.

References

1- K. Lehnertz, F. Mormann, T. Kreuz, R. G. Andrzejak, C. Rieke, P. David, *et al.*, "Seizure prediction by nonlinear EEG analysis," *IEEE Engineering in Medicine and Biology Magazine*, vol. 22, no.1, pp. 57–63, (2003).

2- B. S. Chang, and D. H. Lowenstein., "Epilepsy," *New England Journal of Medicine*, Vol. 349, no. 13, pp. 1257–1266, (2003).

3- J. Bancaud, "Proposal for revised clinical and electroencephalographic classification of epileptic seizures," *Epilepsia*, Vol. 22, no 4, pp. 489 – 501, (1981).

4- Epilepsy | national health portal of India, Last Access Date: 15-June-2023, [online], *Available: https://www.nhp.gov.in/disease/neurological/epilepsy*.

5- Epilepsy | world health organization, Last Access Date: 15-June-2023, [online], *Available:* https://www.who.int/news-room/fact-sheets/detail/epilepsy.

6- P. Satishchandra, N. Santhosh, and S. Sinha, "Epilepsy: Indian perspective," *Annals of Indian Academy of Neurology*, vol. 17, no. 5, pp. 3 (2014).

7- Y. Khan, O. Farooq, and P. Sharma, "Automatic detection of seizure onset in pediatric EEG," *International Journal of Embedded Systems and Applications (IJESA)*, vol. 2, no. 3, pp. 81-89 (2012).

8- O. Faust, U. R. Acharya, H. Adeli, and A. Adeli, "Wavelet-based EEG processing for computer-aided seizure detection and epilepsy diagnosis," *Seizure*, vol. 26, pp. 56 – 64, (2015).

9- V. ZeIjkovic, C. Druzgalski, L. Yequn, C. Jian, Y. Xin, M. Bojic, and P. Mayorga, "Automated pre-ictal phase detection algorithm from EEG signals," *Pan American Health Care Exchanges (PAHCE)*, pp. 1-5, (2013).

10- S. M. Usman, *et al.* "Epileptic seizures prediction using machine learning methods," *Computational and Mathematical Methods in Medicine*, pp. 1–10, (2017), https://doi.org/10.1155/2017/9074759

11- U. R. Acharya, *et al.,* "Automated diagnosis of epileptic EEG using entropies," *Biomedical Signal Processing and Control*, vol.7, no. 4, pp. 401–408, (2012).

12- M. Z. Parvez, and M. Paul, "Epileptic seizure detection by exploiting temporal correlation of electroencephalogram signals," *IET Signal Processing*, vol. 9, no. 6, pp. 467–475, (2015).

13- I. Ullah, M. Hussain, and H. Aboalsamh, "An automated system for epilepsy detection using EEG brain signals based on deep learning approach," *Expert Systems with Applications*, vol. 107, pp. 61–71 (2018).

14- R. Basiri, A. Shariatzadeh, S. Wiebe, and Y. Aghakhani, "Focal epilepsy without interictal spikes on scalp EEG: A common finding of uncertain significance," *Epilepsy Research*, vol. 150, pp. 1–6, (2019).

15- O. Faust, U. R. Acharya, H. Adeli, and A. Adeli, "Wavelet-based EEG processing for computer-aided seizure detection and epilepsy diagnosis," *Seizure*, vol. 26, pp. 56–64 (2015).

16- P. M. J. Van, T. Kind, F. Visser, and V. Lagerburg, "Detecting temporal lobe seizures from scalp EEG recordings: a comparison of various features," *Clinical Neurophysiology*, vol. 116, no. 10, pp. 2480–2489 (2005).

17- J. J. Falco-Walter, I. E. Scheffer, and R. S. Fisher, "The new definition and classification of seizures and epilepsy," *Epilepsy Research*, vol. 139, pp. 73–79, (2018).

18- N. Mohamed, D. Rubin, and T. Marwala, "Detection of epileptiform activity in human EEG signals using Bayesian neural networks," *Neural Information Processing- Letters and Reviews*, vol. 10, no. 1, pp. 1–10, (2006).

19- P. Sun, and W. Zhao, "TSSF-CapsNet: Capsule Network with Temporal-Spectral-Spatial Fusion for EEG-Based Seizure Prediction," *Information Fusion*, 103513, (2025). https://doi.org/10.1016/j.inffus.2025.103513.

20- C. R. Vinutha, *et al. "*Automatic Epilepsy Seizure Classification Using EEG Signals Based on the CNN-LSTM Model," *IET Signal Processing*, vol. 7543401, pp. 14 (2025). https://doi.org/10.1049/sil2/7543401

21- S. Hu, Y. Lai, P. A. Valdes-Sosa, *et al.,* "How do reference montage and electrode setup affect the measured scalp EEG potentials," *Journal of Neural Engineering*, vol. 15, no. 2, pp. 026013, (2018).

22- J. N. Acharya, and V. J. Acharya, "Overview of EEG montages and principles of localization," *Journal of Clinical Neurophysiology*, vol. 36, no. 5, pp. 325–329, (2019).

23- Y. Ishiyama, M. Ebe, I. Homma, *et al.,* "Elimination of EKG artifacts from EEGs recorded with balanced non-

cephalic reference electrode method," *Electroencephalography and Clinical Neurophysiology*, vol. 53, no. 6, pp. 662–665, (1982).

24- M. Sazgar, M. G. Young, "*Overview of EEG, Electrode Placement, and Montages,"* In: *Absolute Epilepsy and EEG Rotation Review*, Springer, pp. 117–125, (2019).

25- E. Louis, L. Frey, J. Britton, *et al.,* "Electroencephalography (EEG): An introductory text and atlas of normal and abnormal findings in adults, children, and infants," *American Epilepsy Society*, Chicago, (2016).

26- H. Jasper, "Report of the committee on methods of clinical examination in electroencephalography," *Electroencephalogram Clinical Neuro-physiology*, vol. 10, pp. 370–375 (1958).

27- C.S. Nayak, and A. Kumar, "EEG Normal Sleep," *Treasure Island*, StatPearls Publishing, (2019).

28- C. Alvarado-Rojas, M. Valderrama, A. Fouad-Ahmed, "Slow modulations of high-frequency activity (40–140hz) discriminate preictal changes in human focal epilepsy," *Scientific Reports*, vol. 4, no. 1, (2014).

29- P. N. Modur, "High frequency oscillations and infra slow activity in epilepsy," *Annals of Indian Academy of Neurology*, vol. 17, no. (S-1), pp. S99, (2014).

30- K. Das, *et al.,* "*Early started hybrid denoising technique for medical images," In Recent Trends in Signal and Image Processing*, Springer, pp. 131–140, (2019).

31- S. V. Ramanan, N. V. Kalpakam, J. S. Sahambi, "A novel wavelet-based technique for detection and de-noising of ocular artifact in normal and epileptic electroencephalogram," *In: (2004) International Conference on Communications, Circuits and Systems*, vol. 2, pp. 1027–1031, (2004).

32- S. Chang, B. Yu, and M. Vetterli, "Adaptive wavelet thresholding for image denoising and compression," *IEEE Transactions on Image Processing*, vol. 9, no. 9, pp. 1532–1546, (2000).

33- S. G. Mallat, "A theory for multiresolution signal decomposition: the wavelet representation," *IEEE Transactions on Pattern Analysis and Machine Intelligence*, vol. 11, no. 7, pp. 674 – 693, (1989).

34- K. Das, M. Maitra, P. Sharma, and M. Banerjee, "Early started hybrid denoising technique for medical images," *In Recent Trends in Signal and Image Processing, S. Bhattacharyya, A. Mukherjee, H. Bhaumik, S. Das, & K. Yoshida (eds.)*, Springer Singapore, vol. 727, pp. 131–140, (2018).

35- K. Das, D. Daschakladar, P. P. Roy, "Epileptic seizure prediction by the detection of seizure waveform from the pre-ictal phase of EEG signal," *Biomedical Signal Processing and Control*, vol. 57, pp. 101720, (2020).

36- L. A. Jeni, J. F. Cohn, and F. De-La-Torre, "Facing imbalanced data–recommendations for the use of performance metrics," *In 2013 Humaine association conference on affective computing and intelligent interaction*, Switzerland: IEEE, pp. 245–251, (2013).

37- P. Swami, B. K. Panigrahi, S. Nara, M. Bhatia, and T. Gandhi, *EEG Epilepsy Datasets*-2016, Access Date: 15-June-2023, [online], *Available* http://rgdoi.net/10.13140/RG.2.2.14280.32006.

38- T. Gandhi, B. K. Panigrahi, M. Bhatia, and S. Anand, "Expert model for detection of epileptic activity in EEG signature," *Expert Systems with Applications*, vol. 37, no. 4, pp. 3513–3520, (2010).

39- T. Gandhi, B. K. Panigrahi, and S. Anand, "A comparative study of wavelet families for EEG signal classification," *Neurocomputing*, vol. 74, no. 17, pp. 3051–3057, (2011).

40- T. K. Gandhi, P. P. Chakraborty, G. G. Roy, and B. K. Panigrahi, "Discrete harmony search based expert model for epileptic seizure detection in electroencephalography," *Expert Systems with Applications*, vol. 39, no. 4, pp. 4055–4062, (2012).

41- P. Swami, T. Gandhi, B.K. Panigrahi, M. Tripathi, and S. Anand, "A novel robust diagnostic model to detect seizures in electroencephalography", *Expert Systems with Applications*, vol. 56, pp. 116—130, (2016).

42- K. Das, S.P. Saha, and K. K. Singh, "Detection of Epileptic Form from Seizure from Pre-Ictal Part of Epileptic EEG Recording," In: *Advances in Systems Analysis, Software Engineering, and High Performance Computing*, IGI Global, pp. 36–49, (2020).

43- S. Panwar, "Single electrode EEG data of healthy and epileptic patients," 2020, *Available:* https://doi.org/10.5281/zenodo.3684992.

44- S. Panwar, S. D. Joshi, A. Gupta, and P. Agarwal, "Automated epilepsy diagnosis using EEG with test set evaluation," *IEEE Transactions on Neural Systems and Rehabilitation Engineering*, vol. 27, no. 6, pp. 1106–1116, (2019).

45- A. L. Goldberger, L. A. N. Amaral, L. Glass, J. M. Hausdorff, P. Ch. Ivanov, R. G. Mark, J. E. Mietus, G. B. Moody, C. K. Peng, H. E. Stanley, "PhysioBank, PhysioToolkit, and PhysioNet", Circulation, vol. 101, pp. e215–e220. (2000).

46- D. Cho, B. Min, J. Kim, and B, Lee, "EEG-based prediction of epileptic seizures using phase synchronization elicited from noise-assisted multivariate empirical mode decomposition," *IEEE Transactions on Neural Systems and Rehabilitation Engineering*, vol. 25, pp. 1309–1318, (2016).

47- H. Khan, L. Marcuse, M. Fields, K. Swann, and B. Yener, "Focal onset seizure prediction using convolutional networks," *IEEE Trans. Biomed. Eng*., vol. 65, pp. 2109–2118 (2018).

48- J. Hellar, N. Erfanian, and B. Aazhang, "Epileptic electroencephalography classification using embedded

dynamic mode decomposition," *Journal of Neural Engineering*, vol. 19, no. 3, pp. 036029, (2022). https://doi.org/10.1088/1741-2552/ac7256

49- C. Li, Y. Zhao, R. Song, X. Liu, R. Qian, and X. Chen, "Patient-specific seizure prediction from electroencephalogram signal via multichannel feedback capsule network," *IEEE Trans. Cogn. Dev. Syst.,* vol. 15, pp. 1360–1370 (2023).

50- S. Y. Shah, H. Larijani, R. M. Gibson, D. Liarokapis, "Epileptic seizure classification based on random neural networks using discrete wavelet transform for electroencephalogram signal decomposition," *Appl Sci*., vol. 14, no. 2: pp. 599, (2024). doi: 10.3390/app14020599

51- P. Kunekar, M. K. Gupta, P. Gaur, "Detection of epileptic seizure in EEG signals using machine learning and deep learning techniques," *J Eng Appl Sci.*, vol. 71, no. 21, (2024), doi: 10.1186/s44147-023-00353-y

52- T. Shawly, A. A. Alsheikhy, Y. Said, *et al.,* "LHAENA: Lightweight Hybrid Attention Ensemble Network Architecture for Epileptic Seizure Detection," *Journal of Disability Research*, vol. 4, no. 3 (2025), https://doi.org/10.57197/jdr-2025-0581

.